Robustness of Yu-Shiba-Rusinov resonances in the presence of a complex superconducting order parameter

Jacob Senkpiel,[1] Carmen Rubio-Verdú,[1,2] Markus Etzkorn,[1] Robert Drost,[1] Leslie M. Schoop,[3] Simon Dambach,[4] Ciprian Padurariu,[4] Björn Kubala,[4] Joachim Ankerhold,[4] Christian R. Ast,[1,*] and Klaus Kern[1,5]

[1]*Max-Planck-Institut für Festkörperforschung, Heisenbergstraße 1, 70569 Stuttgart, Germany*
[2]*CIC nanoGUNE, 20018 Donostia-San Sebastián, Spain*
[3]*Department of Chemistry, Princeton University, Princeton, New Jersey 08544, USA*
[4]*Institut für Komplexe Quantensysteme and IQST, Universität Ulm, Albert-Einstein-Allee 11, 89069 Ulm, Germany*
[5]*Institut de Physique, Ecole Polytechnique Fédérale de Lausanne, 1015 Lausanne, Switzerland*

Robust quantum systems rely on having a protective environment with minimized relaxation channels. Superconducting gaps play an important role in the design of such environments. The interaction of localized single spins with a conventional superconductor generally leads to intrinsically extremely narrow Yu-Shiba-Rusinov (YSR) resonances protected inside the superconducting gap. However, this may not apply to superconductors with more complex, energy-dependent order parameters. Exploiting the Fe-doped two-band superconductor $NbSe_2$, we show that due to the nontrivial relation between its complex-valued and energy-dependent order parameters, YSR states are no longer restricted to be inside the gap. They can appear outside the gap (i.e., inside the coherence peaks), where they can also acquire a substantial intrinsic lifetime broadening. *T*-matrix scattering calculations show excellent agreement with the experimental data and relate the intrinsic YSR state broadening to the imaginary part of the host's order parameters. Our results suggest that nonthermal relaxation mechanisms contribute to the finite lifetime of the YSR states, even within the superconducting gap, making them less protected against residual interactions than previously assumed. YSR states may serve as valuable probes for nontrivial order parameters promoting a judicious selection of protective superconductors.

I. INTRODUCTION

In recent decades, Yu-Shiba-Rusinov (YSR) states [1–3] have been used as local probes to study superconductivity [4], adsorbate-substrate interaction [5], their interplay with the Kondo effect [6], and the properties of the impurity spin states themselves [7]. The interest in YSR states has intensified in recent years as they play a vital role in engineering Majorana bound states [8–10] as well as in studying topological superconductors [11]. In a simple BCS-type *s*-wave superconductor with a real-valued energy-independent order parameter [12], YSR states can exist only inside the superconducting gap, which protects them from interacting with, and decaying into, the quasiparticle continuum [13]. If this gap is void of quasiparticles, only a thermally induced decay into the quasiparticle continuum is possible [14]. Residual quasiparticle interactions could slightly broaden the YSR state [15,16]. The situation is different in a *d*-wave superconductor, where the YSR state is intrinsically expected to have a nonzero lifetime broadening inside the gap owing to its nontrivial order parameter [5,17]. However, as we will show here, the behavior of YSR states changes dramatically even for *s*-wave superconductors if they feature a nontrivial order parameter.

We choose an *s*-wave two-band superconductor with finite interband coupling resulting in complex-valued and energy-dependent order parameters [18,19]. This not only leads to a nontrivial relation between the order parameter and the position of the gap edge but, due to causality [20], also implies imaginary parts in the order parameters, which cannot be trivially removed by a gauge transformation. Effectively, intrinsic decay channels for YSR states emerge. Hence, the interplay between interband coupling and YSR states reveals fundamental properties of superconductors that may be relevant for other unconventional materials.

We explore YSR states in the Fe-doped two-band superconductor $NbSe_2$, which have been well studied in the past [21–34]. Due to interband coupling, a BCS-type band induces superconductivity also in a second band (proximity effect), so that the individual order parameters turn out to be strongly energy dependent. The Fe doping gives rise to YSR states that can be directly observed with a scanning tunneling microscope (STM) for impurities near the surface. In this way, we demonstrate that in this two-band superconductor, the energy of YSR states is no longer restricted to inside the gap but is also found within the quasiparticle continuum. More specifically, those YSR states with stronger magnetic exchange coupling are located within the superconducting gap and have a very small intrinsic lifetime broadening due to reduced relaxation. We can also safely neglect thermally activated relaxation processes for YSR states within the gap [14], as we operate at a base temperature of 15 mK, which is more than two orders of magnitude below the superconducting transition temperature. For a weaker exchange coupling, the

YSR states are located outside of the superconducting gap within the coherence peaks, where they broaden substantially with strong intrinsic relaxation channels to the superconducting host. We demonstrate that the enhanced lifetime broadening is directly related to the proximity-induced complex order parameters. Their imaginary parts are associated with relaxation processes within the superconductor. The interaction of an impurity with the individual bands in the bulk makes these decay channels available to the YSR states. In this way, we not only demonstrate the relevance of intrinsic relaxation channels for a certain class of robust quantum states but also establish YSR states as a probe for the imaginary part of a complex-valued and energy-dependent order parameter.

II. EXPERIMENT

Single crystals of Fe-doped $NbSe_2$ were grown by chemical vapor transport. Powders of Nb and Fe in a ratio of 99.45:0.55 were mixed well and then placed in a quartz tube. Se chips were added in a stoichiometric ratio to yield $Nb_{0.9945}Fe_{0.055}Se_2$. Iodine was used as the transport agent. The sealed tube was heated to $900\,^\circ C$ with a temperature gradient of $75\,^\circ C$ for 3 weeks. The structure and composition of the crystals were confirmed with x-ray diffraction.

Experiments were carried out in a home-built STM operating at 15 mK base temperature. Samples were cleaved using Scotch tape in ultrahigh vacuum. To enhance the experimental resolution, superconducting vanadium was chosen as a tip material [6]. Tips were cut from 0.1-mm vanadium wire (Goodfellow) in air and cleaned by Ar^+ ion sputtering in UHV followed by field emission on a V(100) sample. Tips were characterized on a clean V(100) surface before measurements on $NbSe_2$, and the tip gap was extracted by fitting superconductor-insulator-superconductor (SIS) tunnel spectra while assuming the bulk gap of the vanadium sample was $\Delta_V = 710\,\mu eV$.

III. CHARACTERIZING Fe-DOPED NbSe₂

Layered $NbSe_2$ is a two-band superconductor, whose bands interact via electron hopping between states near the Fermi edge [18,19,23,24,28,29,31,34,35]. We follow the description by McMillan to model this mechanism [19]. Without the interband coupling, the first band is commonly assumed to be superconducting, while the second is not [28]. Only the interband coupling induces superconductivity in the second band, which in turn reduces the order parameter in the first band. As a result, two energy-dependent order parameters emerge, which are complex-valued due to causality [20]. The imaginary part can be interpreted as an intrinsic inverse lifetime due to the hopping between the bands. This stands in contrast to the real-valued energy-independent BCS-type order parameter.

In order to induce YSR states in the $NbSe_2$ host, we have doped the crystal with about 0.55% Fe [36]. Dopants that are close to the surface can be directly seen in the topographic image shown in Fig. 1. We find two characteristic types of impurities in our samples, which we attribute to Fe defects: one with a triangular ($\triangle$) shape [Fig. 1(a)] and one with a W shape [Fig. 1(b)]. Both give rise to strong YSR states, as can be seen in the differential conductance spectra measured with
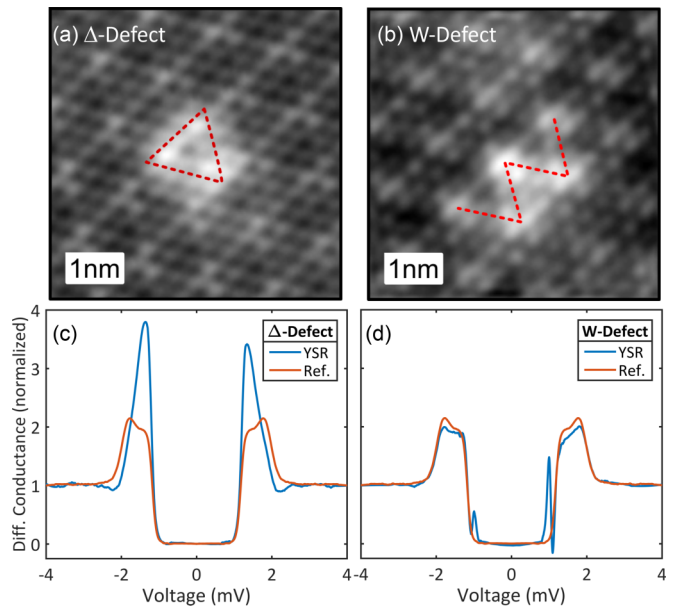

FIG. 1. Topography and differential conductance spectra of Fe in $NbSe_2$: Topographies of the two most common Fe impurities having (a) a triangular shape ($\triangle$) and (b) a W shape (W). (c) The triangular defect typically has a smaller exchange coupling, so that the YSR states appear within the coherence peaks. (d) The W defect typically has a higher exchange coupling, and the YSR states commonly appear inside the gap. An unperturbed reference spectrum with no Fe impurity in the vicinity is shown in red. The current set point for the topography was 20 pA at a bias voltage of 100 mV; the set point for the spectra was 200 pA at 4 mV.

a superconducting vanadium tip in Figs. 1(c) and 1(d), respectively. However, the $\triangle$ defect shows the YSR state inside the coherence peaks [Fig. 1(c)], as can be seen by comparison with the spectrum on the bare surface (red line). Indeed, the asymmetry of the peak heights suggests the existence of YSR states as opposed to a change of the local tunneling probability into the two different bands. By contrast, the YSR state in Fig. 1(d) appears close to the gap edge but clearly inside the gap. Evidently, these two types of YSR states substantially differ in linewidth. The in-gap linewidth [Fig. 1(d)] is much narrower than the line width outside the gap [Fig. 1(c)]. These experimental results present quite a different appearance of YSR states than the "conventional" extremely narrow features occurring only inside the superconducting gap [37]. In the following, we will demonstrate that this is a direct consequence of the energy-dependent order parameter.

Both topographic images in Fig. 1 show a rather regular, continuous lattice corrugation modulated only by a stronger density of states at the defect positions, suggesting that the impurities are buried very close to the surface but not directly at or on the surface. For further analysis, we subtract an unperturbed reference spectrum of the bare surface, i.e., with no impurities in the close vicinity of the YSR state, in order to isolate the YSR states.

IV. THE ORDER PARAMETERS IN Fe-DOPED NbSe₂

In order to find a simple, yet appropriate, theoretical model, we need a detailed description of the order parameter in

Fe-doped $NbSe_2$. The doping of 0.55% of Fe atoms is already strong enough to reduce the transition temperature from about 7.2 K [23,38,39] to 6.1 K [36], so that the effects of the magnetic impurities on the bulk superconductor cannot be neglected. In order to theoretically describe the superconducting order parameter, we have to include the interaction between the two bands [18,19,40], as well as the interaction with a small but finite concentration of magnetic impurities [2,41,42]. As we are analyzing density of states measurements with no momentum information on the band structure or on the order parameter, we refrain from employing models involving momentum-dependent order parameters [22,29,33] and instead focus on an effective description of the order parameter (for details, see the Supplemental Material [36]). We add the self-energies of the two interactions to the bare order parameters $\Delta_{1,2}^{\text{BCS}}$ for the first and second bands, respectively, and find two coupled equations for the two order parameters $\Delta_{1,2}(\omega)$ [43,44]:

$$\Delta_1(\omega) = \Delta_1^{\text{BCS}} - \Gamma_{12}\frac{\Delta_1(\omega) - \Delta_2(\omega)}{\sqrt{\Delta_2^2(\omega) - \omega^2}} - \zeta_1\frac{\Delta_1(\omega)}{\sqrt{\Delta_1^2(\omega) - \omega^2}},$$

$$\Delta_2(\omega) = \Delta_2^{\text{BCS}} - \Gamma_{21}\frac{\Delta_2(\omega) - \Delta_1(\omega)}{\sqrt{\Delta_1^2(\omega) - \omega^2}} - \zeta_2\frac{\Delta_2(\omega)}{\sqrt{\Delta_2^2(\omega) - \omega^2}}.$$

(1)

Here, ω is the energy, Γ_{12} and Γ_{21} are the coupling parameters between the two bands, and $\zeta_{1,2}$ are the coupling constants of the first and second bands to the finite concentration of magnetic impurities. The interband hopping and the impurity interaction are proportional to the density of states $n_{1,2}$ at the Fermi level of each band, so that the parameters in Eq. (1) are related in the following way:

$$\frac{\Gamma_{21}}{\Gamma_{12}} = \frac{\zeta_1}{\zeta_2} = \frac{n_1}{n_2}.$$

(2)

Equation (1) can be solved numerically using a multidimensional Newton-Raphson method. A more detailed discussion of these equations is given in the Supplemental Material [36].

The resulting normalized density of states $\rho_i(\omega)$ of the ith band is

$$\rho_i(\omega) = \text{Re}\left[\frac{\omega}{\sqrt{\omega^2 - \Delta_i^2(\omega)}}\right],$$

(3)

so the total normalized density of states can be written as

$$\rho(\omega) = \frac{1+\eta}{2}\rho_1(\omega) + \frac{1-\eta}{2}\rho_2(\omega),$$

(4)

where η is a ratio that accounts for the different densities of states as well as the different tunneling probabilities into the two bands. Using the total density of states convolved with the superconducting density of states of the V tip and with the energy resolution function [45], we can fit the model to our experimental data. For details, see the Supplemental Material [36].

The resulting fit captures the experimental differential conductance quite accurately, as shown in Fig. 2(a). Following a previous analysis [28], we have assumed a second band
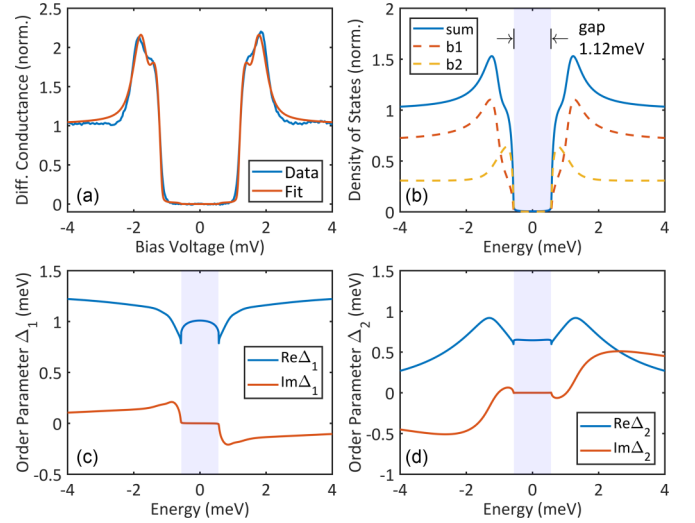

FIG. 2. Extracting the order parameters of Fe-doped $NbSe_2$: (a) Fit of the interband-impurity model to an unperturbed conductance spectrum. The extracted fit parameters provide the input values for the subsequent analysis. (b) Calculated total density of states of the superconducting substrate from the extracted fit parameters (sum). The weighted densities of states for band 1 (b1) and band 2 (b2) are shown as dashed lines. Note that the gap edges of both bands are at the same energy. (c) Resulting order parameter $\Delta_1(\omega)$ of the first band. (d) Resulting order parameter $\Delta_2(\omega)$ of the second band. The blue shaded region indicates the gap.

that is intrinsically normal conducting, $\Delta_2^{\text{BCS}} = 0$. The best fits are obtained for a density of states ratio of $n_1/n_2 = 5$, in agreement with previous assessments [28]. The unperturbed order parameter for the first band $\Delta_1^{\text{BCS}} = 1.27$ meV is somewhat smaller than what has been reported for undoped $NbSe_2$ ($\Delta_1^{\text{BCS,lit}} = 1.4$ meV; see Ref. [28] and references therein) but corresponds to roughly the same ratio as the reduction in the transition temperature from 7.2 to 6.1 K. For the coupling terms, we find $\Gamma_{12} = 0.36$ meV, $\zeta_1 = 57\,\mu\text{eV}$, and $\eta = 0.38$. The extracted density of states of Fe-doped $NbSe_2$ is plotted in Fig. 2(b). The weighted individual densities of states are shown as dashed lines. Their gap edges lie at the same energy. The total density of states (solid line) features rather blunt coherence peaks, where shoulders indicate the coherence peaks of the second band. The gap itself is substantially narrower (1.12 meV) than the bare BCS gap ($2\Delta_1^{\text{BCS}} = 2.54$ meV; see the Supplemental Material [36]). The corresponding order parameters are plotted in Figs. 2(c) and 2(d). For large energies the real part of the order parameter for the first band shows an asymptotic approach to the Δ_1^{BCS} value of 1.27 meV, while the imaginary part approaches zero. Inside the gap, the order parameter is entirely real valued. In the vicinity of the coherence peaks, however, a strong energy dependence is visible. The order parameter of the second band approaches zero for large energies.

As a consequence, it becomes clear that for energies below and around the coherence peaks, the real parts of the order parameters shown in Figs. 2(c) and 2(d) are larger than the energy of the gap edge (± 0.55 meV). Because the energy position of the YSR state is directly related to the value of

the order parameter, we can already anticipate unconventional locations of the YSR states [17,46].

V. MAGNETIC IMPURITY SCATTERING OF Fe IN NbSe₂

We now turn to the impurity scattering and calculate the YSR spectra following a simple T-matrix scattering formalism [17]. We follow a mean-field approach in assuming that the $\zeta_{1/2}$ terms affect the sample density of states (DOS) on a global scale, while YSR scattering is local. The superconducting host is described by the normalized Green's function for the two bands $G_{1,2}(\omega)$ using the energy-dependent order parameters discussed in the previous section:

$$G_{1,2}(\omega) = -\pi \frac{1 \pm \eta}{2} \frac{(\omega + i\Gamma)\sigma_0 - \Delta_{1,2}(\omega)\sigma_1}{\sqrt{\Delta_{1,2}^2(\omega) - (\omega + i\Gamma)^2}}. \quad (5)$$

Here, σ_i are the Pauli matrices in Nambu space, with σ_0 being the identity matrix. We add a Dynes-type parameter $\Gamma \leqslant 5\,\mu$eV as a phenomenological lifetime broadening [15]. Larger values of Γ fill the gap, which is not observed in the experiment. The T matrix for the ith band can be written as

$$T_i(\omega) = V_i[1 - G_i(\omega)V_i]^{-1}, \quad V_i = J_i'\sigma_0 + U_i'\sigma_3, \quad (6)$$

where V_i is the scattering potential, with $J_i' = \frac{1}{2}JSn_i$ being the dimensionless, effective magnetic exchange coupling and $U_i' = Un_i$ being the dimensionless, effective local Coulomb scattering. Furthermore, $\frac{1}{2}JS$ is the exchange coupling of a classical spin, U is the local Coulomb potential, and n_i is the density of states of the ith band at the Fermi level. The total Green's function $G_i^{\text{YSR}}(\omega)$ can be written as

$$G_i^{\text{YSR}}(\omega) = G_i(\omega) + G_i(\omega)T_i(\omega)G_i(\omega). \quad (7)$$

For simplicity we consider only the total Green's function at the position of the impurity. Inserting the energy-dependent order parameters into Eq. (5), we can calculate the spectral function $A_i(\omega) = -\frac{1}{\pi}\text{tr}\{\text{Im}[G_i^{\text{YSR}}(\omega)]\}$ and thus the density of states of the YSR resonances for different exchange couplings J_i'.

The calculated YSR resonances for different exchange couplings $J_1' = (n_1/n_2)J_2'$ are plotted in Fig. 3. For weak exchange coupling, the YSR state interacting with the first band can be found within the coherence peaks [see Fig. 3(a)]. For stronger exchange coupling (but still below the zero-energy crossing [6]), the YSR state for the first band moves into the gap and becomes extremely sharp, as can be seen in Fig. 3(b). Inside the gap, the width of the YSR state is given by the parameter Γ. In Figs. 3(c) and 3(d), the YSR spectra are shown as a function of exchange coupling J' for the first and second bands, respectively. With increasing coupling to the first band, the YSR peaks shift towards zero energy and become extremely narrow when entering the gap region.

Apparently, the second band affects the YSR states much less, as can be seen in Figs. 3(c) and 3(d). Both bands have predominantly Nb d character [29,31]. However, as the effective exchange coupling between the impurity and the superconductor is proportional to the density of states in the superconductor, i.e., $J_1'/J_2' = n_1/n_2$, we may assume
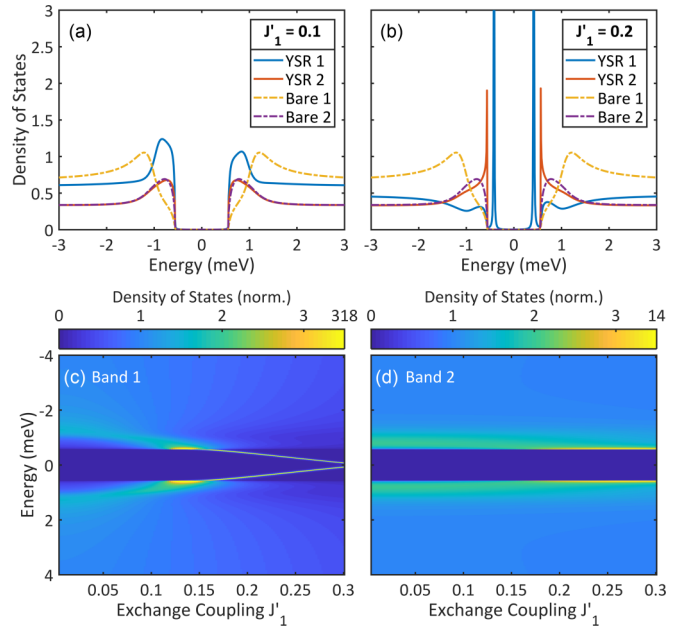

FIG. 3. Calculated YSR states: The solid lines correspond to the YSR spectra coupling to band 1 (YSR 1) and band 2 (YSR 2), while the dashed lines represent the unperturbed spectra for the first (bare 1) and second (bare 2) bands, respectively. The ratio between the spectra of the two bands corresponds to the typical ratio η observed in the experiment. A small value for the Coulomb interaction $U_1' = 0.05$ and $U_2' = 0.01 = U_1'n_2/n_1$ was chosen to make the spectrum asymmetric. (a) YSR spectrum for weak exchange coupling. The YSR state is broad and within the region of the coherence peaks. (b) Stronger coupling than in (a), but still before the zero-bias crossing. The YSR state resides within the gap and has become extremely sharp. (c) and (d) YSR spectra vs exchange coupling in band 1 and band 2, respectively. The color scaling is adapted to show the weaker features; it is nonlinear for values larger than 3.5. The sharpening of the peak as it enters the gap is clearly visible. In (d) the YSR peak develops much slower due to the reduced density of states in band 2. For all panels, $J_1'/J_2' = n_1/n_2$.

a strongly reduced impact of the second band. We therefore consider in leading order only the YSR resonances in the first band.

Due to the complicated shape of the YSR spectra, we restrict the following analysis of the peaks to the peak position and full width at half maximum. These quantities provide direct insight into the nature of the YSR state-bulk interaction. Keeping in mind that the peak position directly depends on the strength of the exchange coupling (Fig. 3), the extracted values are displayed in Fig. 4(a), where the color coding represents the strength of the exchange coupling J'. The red line in Fig. 4(a) shows twice the imaginary part of the order parameter of the first band $|2\text{Im}\Delta_1(\omega)|$.

We observe a clear correlation between the broadening of the peak and the emergence of a finite $\text{Im}\Delta_1(\omega)$ as calculated from Eq. (1). When the YSR peak position approaches the coherence peaks, where $|\text{Im}\Delta_1(\omega)|$ increases abruptly, their width increases abruptly as well. Thus, there is a clear indication that the width of a YSR peak is related to the imaginary part of the superconducting order parameter.
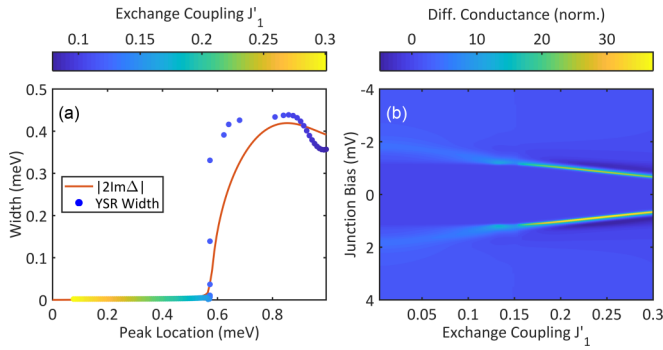
FIG. 4. Evolution of the YSR peak width: (a) YSR peak width vs peak location. The width becomes extremely narrow in the region of the superconducting gap. The color coding represents the strength of the exchange coupling. The red line is twice the imaginary part of the order parameter $\Delta_1(\omega)$ of the first band. We see a clear correlation between the peak width and the imaginary part. (b) Differential conductance calculated from the YSR spectral function and the density of states of the superconducting V tip as well as finite energy resolution. The sharpening of the YSR state when entering the gap is clearly visible.

VI. DISCUSSION

In order to correlate the experimentally observed broadening of the YSR peak and its position with theory, we calculate the differential conductance from the density of states following Eq. (7). The resulting spectra are shown in Fig. 4(b) as a function of exchange coupling J_1'. The sharpening of the peaks when entering the region of the gap is clearly visible even though the width of the YSR peaks is now limited by the energy resolution of the STM [45]. Two representative spectra of YSR states outside and inside the gap are plotted in Figs. 5(a) and 5(b), respectively. An unperturbed, averaged reference spectrum was subtracted to suppress the coherence peaks and isolate the YSR states. These experimental spectra can be compared to Figs. 5(c) and 5(d), showing two slices from Fig. 4(b) with similar peak positions as in Figs. 5(a) and 5(b), respectively. The calculated spectra are normalized to the normal-state conductance and scaled with the ratio η [see Eq. (4)]. The subtraction of an unperturbed reference spectrum is not necessary in the calculated spectra because the coherence peaks are inherently suppressed at the impurity center where the DOS is calculated. Selecting theoretical spectra with matching peak positions, we observe good agreement between the corresponding panels concerning the width of the YSR peaks as well as their overall shape. We find, however, a reduced height in the experimental peaks, which we attribute to the measurement slightly above the (subsurface) impurity. Away from the scattering center of the impurity, intensity modulations can strongly reduce the peak height [30]. We assume that they do not affect the peak position or their width. Interestingly, the asymmetry of the YSR peaks is different in Figs. 5(a) and 5(b), which indicates a different Coulomb scattering potential U' (assuming that the particle-hole asymmetry in the lattice Green's function does not change significantly between the impurities).

From each of the experimental and theoretical spectra, we extract the YSR peak widths and positions as indicated in Figs. 5(a)–5(d) and display them in Fig. 5(e). Excellent agree-
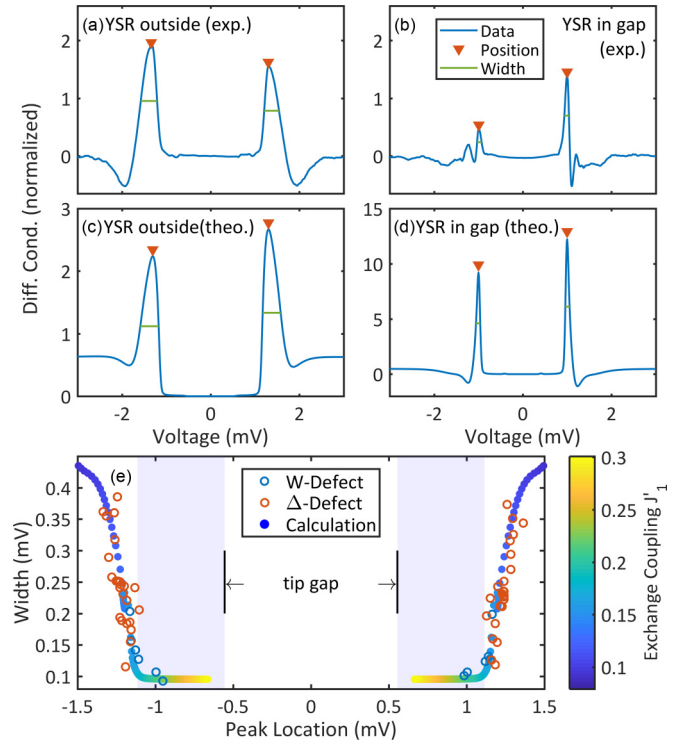

FIG. 5. Comparison of experiment with theory: Peak positions and widths indicated for YSR states (a) outside the gap and (b) inside the gap, where an unperturbed reference spectrum was subtracted. (c) and (d) The corresponding calculated spectra. (e) Experimental YSR peak widths vs peak position in comparison with the extracted YSR peak widths from the calculated differential conductance spectra. The W-shaped defect and the triangular defect (Δ) are color-coded in blue and red, respectively. The blue shaded region indicates the sample gap.

ment is seen between the experimentally extracted values and the calculated spectra, indicating that there is indeed a strong correlation between the shape and position of the YSR states and the details of the underlying order parameter. Although W defects seem to couple stronger than Δ defects, both defects can be found in a range of exchange couplings (probably due to slightly different local environments), such that either defect can be used independently to infer the relation of the width to the imaginary part of the order parameter.

In a regular s-wave BCS superconductor the order parameter defines the position of the gap edge. YSR states must then always lie within the gap. Interband coupling in a multiband superconductor leads to energy-dependent Δ_1, which necessarily has a nonzero imaginary part [20]. The gap edge no longer corresponds to the value of Δ_1 in this case and is generally found at lower energies. YSR states may then be found within the coherence peaks but still at energies smaller than Δ_1. We observe a marked increase in the linewidth of YSR states when they overlap with the coherence peaks.

The spectral functions on which these arguments are based result from the imaginary parts of respective Green's functions, which are commonly interpreted as single-particle excitation spectra. The widths of the calculated features are determined by their relaxation rate into the ground state. The imaginary part of the order parameter can then be interpreted

as a measure for the effective lifetime of YSR bound states. Indeed, an imaginary Δ_1 renders the Green's function considered here non-Hermitian and indicates energy dissipation. These relaxation processes are strongest for YSR states located within the coherence peaks where the order parameter has a finite imaginary part. They sharpen up considerably within the superconducting gap, where the imaginary part of the order parameter tends to zero and there are few relaxation channels. The experimental linewidth is then limited by the resolution of our STM, which is determined by the interaction of the tunneling quasiparticles with the local electromagnetic environment according to the $P(E)$ description [45,47,48].

This finite energy resolution of the STM obscures a direct observation of the peak width inside the superconducting gap. The full width at half maximum of the energy resolution function is dominated by the fluctuations of single charges at the junction capacitance [45] and is usually much broader than the intrinsic peak width of just a few μeV. Nevertheless, we surmise that even in the gap, there can be weak couplings to inelastic relaxation processes, which may be modeled effectively by a generic imaginary constant self-energy, such as the Dynes parameter [15].

The correlation between YSR linewidth and Im$\Delta_1(\omega)$ suggests that YSR states can also be exploited as local probes capable of measuring the imaginary part of a superconducting order parameter. A quantitative analysis would need to explicitly include the local modifications of the order parameter induced by the YSR states themselves [17,49]. The nature and symmetry of the superconducting order parameter remain a subject of much debate across a wide field of materials in the scientific literature. Using YSR states as probes for the complex part of the superconducting order parameter could give valuable insight into the superconductivity of other nontrivial materials, especially those of an unconventional, proximity-induced, or topological nature.

VII. CONCLUSION

In summary, we have shown that complex-valued energy-dependent order parameters as they can result from multiband superconductivity give rise to nontrivial interactions with local pair-breaking potentials. The resulting YSR states may not just exist in the superconducting gap and can also overlap with the coherence peaks. In the latter case, they acquire a substantial linewidth due to dissipative relaxation processes into the continuum. These processes are expressed in the order parameter, which can be interpreted as a "rephrased" self-energy. We show that the imaginary part of the order parameter is connected to lifetime broadening. Our analysis focused on the two-band s-wave superconductor NbSe$_2$ as a model system. We expect similar or even more complex interactions of YSR states with unconventional (d-wave, p-wave), proximity-induced, and/or topological superconductors. At the same time, we have demonstrated that YSR states may serve as sensitive probes for the imaginary part of the order parameter, which opens up new possibilities for understanding the intricacies of multiband superconductivity as well as unconventional superconductors through the study of pair-breaking potentials.

[1] L. Yu, Acta Phys. Sin. **21**, 75 (1965).
[2] H. Shiba, Prog. Theor. Phys. **40**, 435 (1968).
[3] A. I. Rusinov, Zh. Eksp. Teor. Fiz. Pis'ma Red. **9**, 146 (1968) [JETP Lett. **9**, 85 (1969)].
[4] A. Yazdani, B. A. Jones, C. P. Lutz, M. F. Crommie, and D. M. Eigler, Science **275**, 1767 (1997).
[5] E. W. Hudson, K. M. Lang, V. Madhavan, S. H. Pan, H. Eisaki, S. Uchida, and J. C. Davis, Nature (London) **411**, 920 (2001).
[6] K. J. Franke, G. Schulze, and J. I. Pascual, Science **332**, 940 (2011).
[7] M. Ruby, Y. Peng, F. von Oppen, B. W. Heinrich, and K. J. Franke, Phys. Rev. Lett. **117**, 186801 (2016).
[8] S. Nadj-Perge, I. K. Drozdov, B. A. Bernevig, and A. Yazdani, Phys. Rev. B **88**, 020407(R) (2013).
[9] S. Nadj-Perge, I. K. Drozdov, J. Li, H. Chen, S. Jeon, J. Seo, A. H. MacDonald, B. A. Bernevig, and A. Yazdani, Science **346**, 602 (2014).
[10] M. Ruby, F. Pientka, Y. Peng, F. von Oppen, B. W. Heinrich, and K. J. Franke, Phys. Rev. Lett. **115**, 197204 (2015).
[11] G. C. Ménard, S. Guissart, C. Brun, R. T. Leriche, M. Trif, F. Debontridder, D. Demaille, D. Roditchev, P. Simon, and T. Cren, Nat. Commun. **8**, 2040 (2017).
[12] A. V. Balatsky, I. Vekhter, and J.-X. Zhu, Rev. Mod. Phys. **78**, 373 (2006).
[13] B. W. Heinrich, L. Braun, J. I. Pascual, and K. J. Franke, Nat. Phys. **9**, 765 (2013).
[14] M. Ruby, F. Pientka, Y. Peng, F. von Oppen, B. W. Heinrich, and K. J. Franke, Phys. Rev. Lett. **115**, 087001 (2015).
[15] R. C. Dynes, V. Narayanamurti, and J. P. Garno, Phys. Rev. Lett. **41**, 1509 (1978).
[16] I. Martin and D. Mozyrsky, Phys. Rev. B **90**, 100508(R) (2014).
[17] M. I. Salkola, A. V. Balatsky, and J. R. Schrieffer, Phys. Rev. B **55**, 12648 (1997).
[18] H. Suhl, B. T. Matthias, and L. R. Walker, Phys. Rev. Lett. **3**, 552 (1959).
[19] W. L. McMillan, Phys. Rev. **175**, 537 (1968).
[20] J. S. Toll, Phys. Rev. **104**, 1760 (1956).
[21] H. F. Hess, R. B. Robinson, and J. V. Waszczak, Phys. Rev. Lett. **64**, 2711 (1990).
[22] N. Hayashi, M. Ichioka, and K. Machida, Phys. Rev. B **56**, 9052 (1997).
[23] T. Yokoya, T. Kiss, A. Chainani, S. Shin, M. Nohara, and H. Takagi, Science **294**, 2518 (2001).

[24] J. Rodrigo and S. Vieira, Phys. C (Amsterdam, Neth.) **404**, 306 (2004).

[25] A. Kohen, T. Proslier, T. Cren, Y. Noat, W. Sacks, H. Berger, and D. Roditchev, Phys. Rev. Lett. **97**, 027001 (2006).

[26] I. Guillamon, H. Suderow, F. Guinea, and S. Vieira, Phys. Rev. B **77**, 134505 (2008).

[27] H. Kimura, R. P. Barber, S. Ono, Y. Ando, and R. C. Dynes, Phys. Rev. B **80**, 144506 (2009).

[28] Y. Noat, T. Cren, F. Debontridder, D. Roditchev, W. Sacks, P. Toulemonde, and A. San Miguel, Phys. Rev. B **82**, 014531 (2010).

[29] D. J. Rahn, S. Hellmann, M. Kalläne, C. Sohrt, T. K. Kim, L. Kipp, and K. Rossnagel, Phys. Rev. B **85**, 224532 (2012).

[30] G. C. Ménard, S. Guissart, C. Brun, S. Pons, V. S. Stolyarov, F. Debontridder, M. V. Leclerc, E. Janod, L. Cario, D. Roditchev, P. Simon, and T. Cren, Nat. Phys. **11**, 1013 (2015).

[31] Y. Noat, J. A. Silva-Guillén, T. Cren, V. Cherkez, C. Brun, S. Pons, F. Debontridder, D. Roditchev, W. Sacks, L. Cario, P. Ordejón, A. García, and E. Canadell, Phys. Rev. B **92**, 134510 (2015).

[32] A. Ptok, S. Glodzik, and T. Domanski, Phys. Rev. B **96**, 184425 (2017).

[33] J. A. Galvis, E. Herrera, C. Berthod, S. Vieira, I. Guillamon, and H. Suderow, Commun. Phys. **1**, 30 (2018).

[34] T. Dvir, F. Massee, L. Attias, M. Khodas, M. Aprili, C. H. L. Quay, and H. Steinberg, Nat. Commun. **9**, 598 (2018).

[35] K. Machida and F. Shibata, Prog. Theor. Phys. **47**, 1817 (1972).

[36] See Supplemental Material at http://link.aps.org/supplemental/10.1103/PhysRevB.100.014502 for details on sample preparation and characterization as well as data analysis.

[37] B. W. Heinrich, J. I. Pascual, and K. J. Franke, Prog. Surf. Sci. **93**, 1 (2018).

[38] R. F. Frindt, Phys. Rev. Lett. **28**, 299 (1972).

[39] E. Revolinsky, G. A. Spiering, and D. J. Beerntsen, J. Phys. Chem. Solids **26**, 1029 (1965).

[40] N. Schopohl and K. Scharnberg, Solid State Commun. **22**, 371 (1977).

[41] A. A. Abrikosov and L. P. Gor'kov, J. Exp. Theor. Phys. (U.S.S.R.) **39**, 480 (1960) [Sov. Phys. JETP **12**, 337 (1961)].

[42] K. Maki, Prog. Theor. Phys. **32**, 29 (1964).

[43] H. G. Zarate and J. P. Carbotte, J. Low Temp. Phys. **59**, 19 (1985).

[44] A. A. Golubov and I. I. Mazin, Phys. Rev. B **55**, 15146 (1997).

[45] C. R. Ast, B. Jäck, J. Senkpiel, M. Eltschka, M. Etzkorn, J. Ankerhold, and K. Kern, Nat. Commun. **7**, 13009 (2016).

[46] M. E. Flatte and J. M. Byers, Phys. Rev. B **56**, 11213 (1997).

[47] M. H. Devoret, D. Esteve, H. Grabert, G.-L. Ingold, H. Pothier, and C. Urbina, Phys. Rev. Lett. **64**, 1824 (1990).

[48] D. Averin, Y. Nazarov, and A. Odintsov, Phys. B (Amsterdam, Neth.) **165-166**, 945 (1990).

[49] M. E. Flatte and J. M. Byers, Phys. Rev. Lett. **78**, 3761 (1997).